

Nanostructured Carbon Catalyst for Amide Coupling Reactions under Microwave Heating in the Absence of a Solvent

Damian Pawelski, Olivia Fernandez Delgado, Agnieszka Z. Wilczewska, Jakub W. Strawa, and Marta E. Plonska-Brzezinska*



Cite This: *ACS Appl. Nano Mater.* 2022, 5, 16376–16387



Read Online

ACCESS |



Metrics & More



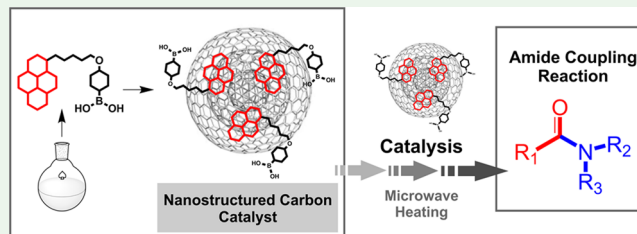
Article Recommendations



Supporting Information

ABSTRACT: Carbon nanostructures offer a perfect link between nanoscale materials and organic molecules, making them an ideal platform for molecular catalysts. Herein, an efficient, straightforward, and high-yield synthetic approach is described to synthesize aryl boronic acid containing the pyrene moiety that is non-covalently immobilized by π - π interaction to carbon nano-onions' surface. The nanostructured carbon material catalyzes the direct amide coupling reaction under microwaved heating in the absence of a solvent. The multilayered structures of carbon nano-onions ensure high thermal stability, and simultaneously, they are excellent microwaved absorbers, which reduce energy consumption. The absorption of microwaved radiation by the nanostructured carbon catalyst effectively influences yield of the catalytic reaction, which is up to 94%. Additionally, the recovery of catalytic material is straightforward, and the mass losses are negligible. Microwave heating in a solvent-free condition simplifies the reaction and reduces the amount of waste, which, in turn, depletes the environmental impact.

KEYWORDS: nanostructured carbon catalyst, microwave-assisted synthesis, carbon nano-onion, heterogeneous catalysis, amide coupling reaction, microwave heating



1. INTRODUCTION

The formation of an amide bond is an essential issue in synthetic chemistry as it is a structural part of commonly used chemical compounds.¹ For example, it has been estimated that up to 25% of all synthetic pharmaceuticals contain at least one amide bond.² Amide synthesis is often accomplished by condensation between amines and carboxylic acids. This reaction does not occur spontaneously, and it requires heating to high temperatures, in which a water molecule is released (>160 °C). It is postulated that the high energy barrier of the condensation reaction is related to the formation of an organic salt after mixing the reactants, which is formed as a result of an exothermic neutralization reaction. Therefore, the appearance of the amide bond requires a more complex molecular rearrangement, with the simultaneous separation of the water molecule. Direct thermal reaction of amide condensation is not a feasible strategy for many substrates because sensitive functional groups do not survive under such harsh conditions.³ Additionally, the reactants should have specific properties, such as melting points below 200 °C, low volatility, and high thermal stability.^{3,4}

Many commercially available reagents allow the direct amide coupling reaction to be carried out under milder conditions than those resulting from the thermal method. The most important types of coupling reagents include carbodiimides, compounds generating carbonic anhydrides, triazine-based,

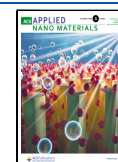
phosgene derivatives, etc.¹ A method of SO_2F_2 -mediated direct clickable coupling of carboxylic acids with amines was reported as a highly efficient way to synthesize amides.^{5,6} *N*-Aryl amides directly from nitroarenes and carboxylic acids as coupling substrates⁷ and catalytic direct amidation reaction using *tert*-butyl acetate as the reaction solvent were also performed.⁸ Usage of these reagents can simultaneously generate additional post-reaction waste. This fact becomes particularly troublesome when a large-scale synthesis of pharmaceuticals is carried out. Low efficiencies and applicability of the thermal process, as well as high costs and unfavorable atomic economy of other methods, make the issue of amide coupling an attractive direction of scientific research.

Overcoming the high energy barrier of the direct amidation reaction can be effectively supported by microwave heating (MW). This experimental condition allows proceeding the reaction faster, more cleanly, and with higher yields than similar reactions under conventional heating.^{9,10} The mechanism of MW heating differs according to the interaction

Received: August 5, 2022

Accepted: October 24, 2022

Published: November 7, 2022



between the MW and substrate. It is mainly based on the interfacial and dipolar polarization of the components and the movement of charged particles that generate heat from collisions.¹¹ Several direct amidation reaction methods have been developed involving MW heating and the catalyst additives, such as *p*-toluenesulfonic acid, zeolite-HY, KF-alumina, silica gel, K-10 montmorillonite, and others.¹² One of the more desirable strategies is catalytic methods, e.g., boron compounds (boric acid,¹³ aryl boronic acids,^{14,15} alkyl boronic acid,¹⁶ boric acid esters,⁸ etc.) and transition-metal salts (Zn,¹⁷ Cr,¹⁸ Pd,¹⁹ etc.) as well as enzymes.²⁰ Although high reaction yields can be obtained with catalysts, they also have some limitations. The disadvantages of catalytic methods include the problem of catalyst renewal, time of reaction, high solvent consumption, and the presence of metallic impurities in the product.²¹

Renewable aryl boronic acidic catalysts made direct amidation condensation more environmentally friendly and efficient.^{22,23} Most of the proposed solutions presented in the literature include the covalent immobilization of aryl boronic acid on a polystyrene resin^{22,24} and silica gel.²³ The catalysts were also recovered from the post-reaction mixture using basic isolation techniques.²⁵ The advantage of a solid-carrier catalyst is the possibility of its simple recovery from the reaction mixture.

Carbon nanomaterials are frequently used, given their wide availability, environmental acceptability, and unique surface properties. Currently, they are attractive candidates for catalytic materials and their carriers.²⁶ The strategy of noncovalent functionalization of carbon nanomaterials with pyrene compounds was successfully used for immobilization of enzymes,²⁷ 2,2,6,6-tetramethyl-1-piperidinyloxy (TEMPO) derivatives,²⁸ the S_N2 reaction catalyst,²⁹ metallic complexes of Mn,³⁰ Cu,³¹ Fe,³² Pd,³³ and Rh.³⁴

Carbon nano-onions (CNOs) are zero-dimensional carbon nanoparticles with a multilayer spherical graphite structure with a diameter of 1.4–50 nm due to the different preparation methods.³⁵ The most popular method of obtaining CNO is currently thermal annealing of nanodiamonds, which leads to obtaining nanoparticles of small size (diameter in the range of 5–6 nm) and high reactivity.³⁵ The large graphite surface of CNO (with sp²-hybridized C atoms) enables the formation of supramolecular systems through electrostatic, van der Waals, and π - π interactions.³⁶ Other advantages of using the CNO as catalyst support are the high thermal stability and generally low reactivity toward the components of the possible catalyzed reaction. Additionally, CNO is an excellent MW absorber due to its multilayer graphite structure.³⁷ Therefore, CNO can be a beneficial additive when the remaining components of the reaction mixture poorly absorb MW radiation, like in our case. The unique combination of high electrical conductivity (comparable to carbon black), large external surface area, and nanoscopic size, plus the possibility for large-scale synthesis and chemical modification,³⁸ have made this material very attractive for our applications, ranging from electrochemical energy storage^{39–41} and electrocatalysis^{42,43} to biomedicine.^{44,45}

As part of our ongoing research on the CNO nanostructures, we report the first heterogeneous nanostructured carbon catalysts for the direct amide coupling reaction. However, several articles have been published to indicate the feasibility of using these carbon nanostructures in heterogeneous catalysis.^{46,47} To the best of our knowledge, the CNO nanostruc-

tures have not been used as catalyst support for this type of reaction. Our main goal was to obtain a renewable nanostructured carbon catalyst and to develop a microwave amidation procedure that would require heating for a short period of time. Additionally, MW heating in a solvent-free condition simplifies the reaction and reduces the amount of waste and energy consumption which, in turn, depletes the environmental impact.

2. EXPERIMENTAL SECTION

2.1. Materials. All inorganic reagents were purchased from ChemPure (Poland) and used without pre-purification. All used solvents were purchased from POCH (Poland). Tetrahydrofuran (THF) was dried by distillation from sodium-benzophenone ketyl under Ar. Dimethylformamide (DMF) was dried by vacuum fractional distillation over phosphorus pentoxide and stored in the presence of 3 Å molecular sieves. Toluene, benzene, hexane, heptane, ethyl acetate, dichloromethane (DCM), and chloroform were purified by fractional distillation before use. All air-sensitive reactions were carried out under Ar and in flame-dried reaction vessels. The synthesis of CNO (6–8 shells) was performed by annealing nanodiamonds of 5 nm average particle size under a positive pressure of helium at 1650 °C.⁴⁸

2.2. Synthetic Procedures. **2.2.1. Procedures for Synthesis of Amidation Catalyst.** **2.2.1.1. Preparation of 1-Bromopyrene (1).** To pyrene (36.01 g, 178.0 mmol), *N*-bromosuccinimide (34.86 g, 195.8 mmol, 1.1 equiv), and anhydrous DMF (400 mL) were added.⁴⁹ Lauroyl peroxide (Luperox) (0.71 g, 1.78 mmol, 1 mol %) was then added, and stirring was continued at the set temperature for 48–60 h. Next, 500 mL of 10% Na₂S₂O₃ solution was added to the reaction mixture, and the resulting milky suspension was stirred vigorously for 5 min. After cooling the suspension to room temperature (RT), the precipitate was filtered off. Next, the residue was dissolved in hot toluene (ca. 500 mL), and the resulting solution was dried with anhydrous MgSO₄. The dried solution was filtered through a filter paper and concentrated on a rotary evaporator until the volume allowed for crystallization (approx. 180–200 mL). The solution was left for several hours for spontaneous crystallization. Then, 43.77 g of 1-bromopyrene (**1**) was obtained as a cream solid (87%). R_f (toluene/hexane: 2:5, v/v; 1-bromopyrene) = 0.81; R_f (toluene/hexane: 2:5, v/v; pyrene) = 0.69. mp: 103.1–104.1 °C (toluene). ¹H NMR (500 MHz, DMSO-*d*₆), δ [ppm]: 8.35 (br s, 1H), 8.33 (br s, 1H), 8.32–8.28 (m, 3H), 8.21 (d, *J* = 8.9 Hz, 1H), 8.18 (d, *J* = 8.2 Hz, 1H), 8.15 (br s, 1H), 8.11 (t, *J* = 7.6 Hz, 1H). ¹³C NMR (126 MHz, DMSO-*d*₆), δ [ppm]: 130.6, 130.3, 130.1, 129.4, 128.7, 127.8, 127.0, 127.0, 126.1, 125.8, 125.0, 123.0, 118.9. Fourier transform infrared (FTIR) (KBr), ν [cm⁻¹]: 3033, 2170, 1876, 1374, 1875, 1734, 1723, 1656, 1582, 1529, 1471, 1427, 1237, 1197, 1173, 1075, 1010, 959, 832, 745, 703.

2.2.1.2. Preparation of 1-(5-Bromopentyl)pyrene (2). To compound **1** (6.00 g, 21.36 mmol) anhydrous THF (250 mL) was added. After mixing the components, the solution was cooled with an isopropanol/dry ice bath to -78 °C, and then *n*-BuLi (9.39 mL of a 2.5 M hexane solution, 23.49 mmol, 1.1 equiv) was added dropwise.⁵⁰ The formation of an intensely yellow suspension was observed during the addition of *n*-BuLi. The flask contents were vigorously stirred for 1.5 h at -78 °C, followed by the addition of 0 °C-cooled 1,5-dibromopentane (24.54 g (14.54 mL), 106.8 mmol, 5.0 equiv). An oily crude product was obtained, which also contained unreacted 1,5-dibromopentane. 1,5-Dibromopentane was removed from the product by co-azeotroping distillation with water (65 °C, 80 mBa). The crude product changed from a dark yellow oil to a cream solid. Then toluene (100–150 mL) was added, and the resulting solution was dried with anhydrous Na₂SO₄, filtered, and concentrated to a crystallization volume (ca. 30 mL). The concentrated solution was left for crystallization at approximately -5 °C. The 1-(5-bromopentyl)pyrene (**2**) was obtained as a white solid (7.51 g, 84%). R_f (toluene/hexane: 2:5, v/v) = 0.59. mp: 119.2–120.2 °C (toluene). ¹H NMR (400 MHz, CDCl₃), δ [ppm]: 8.26 (d, *J* = 9.3 Hz, 1H), 8.20–8.18 (m, 4H), 8.04–7.99 (m, 3H), 7.84 (d, *J* = 7.8 Hz,

1H), 3.43 (t, $J = 7.6$ Hz, 2H), 3.34 (m, 2H), 1.96–1.88 (m, 4H), 1.64–1.60 (m, 2H). ^{13}C NMR (101 MHz, CDCl_3), δ [ppm]: 136.7, 131.5, 131.0, 129.9, 128.7, 127.6, 127.3 (d), 126.7, 125.9, 125.2 (d), 125.0, 124.9, 124.8, 123.4, 33.9, 33.4, 32.8, 31.3, 28.4. DEPT 90 (101 MHz, CDCl_3), δ [ppm]: 127.6, 127.3 (d), 126.7, 125.9, 125.0, 124.9, 124.8, 123.4. DEPT 135 (101 MHz, CDCl_3), δ [ppm]: 127.6, 127.3, 126.7, 125.9, 125.0, 124.9, 124.8, 123.4, 33.9, 33.4, 31.1, 28.4. FTIR (KBr), $[\text{cm}^{-1}]$: 3050, 2911, 2841, 2043, 1915, 1781, 1585, 1481, 1236, 1169, 1035, 831, 170, 632, 503. High-resolution mass spectrometry (HRMS) (electrospray ionization (ESI)): calcd m/z : 350.0664, found m/z : 350.0665.

2.2.1.3. Preparation of 1-(5-(4-Bromophenoxy)pentyl)pyrene (3). To 4-bromophenol (4.92 g, 28.47 mmol, 2.0 equiv), NaOH (1.71 g, 42.70 mmol, 3.0 equiv), and anhydrous DMF (100 mL) were added. The flask contents were stirred magnetically until the mixture was clear, and then 1-(5-bromopentyl)pyrene (5.00 g, 14.23 mmol) was added. The flask was closed with a septum, and an Ar balloon was adapted to it and stirred magnetically at 120 °C overnight. Next, the reaction mixture was poured into a separating funnel, and AcOEt (300 mL) and 1 M NaOH solution (200 mL) were added. 5-(4-Bromophenoxy)pentylpyrene was obtained as a white solid (5.76, 91%). R_f (toluene/hexane: 2:5, v/v) = 0.47. mp: 101.0–103.0 °C. ^1H NMR (400 MHz, CDCl_3), δ [ppm]: 8.28 (d, $J = 9.2$ Hz, 1H), 8.20–8.17 (m, 2H), 8.14–78.10 (m, 2H), 8.05–8.00 (m, 3H), 7.87 (d, $J = 7.8$ Hz, 1H), 6.75 (d, $J = 8.9$ Hz, 2H), 3.87 (t, $J = 7.6$ Hz, 2H), 3.37 (t, $J = 7.7$ Hz, 2H), 1.95–1.91 (m, 1H), 1.86–1.82 (m, 2H), 1.65–1.59 (m, 2H). ^{13}C NMR (101 MHz, CDCl_3), δ [ppm]: 158.3, 136.9, 132.3, 131.6, 131.0, 129.9, 128.7, 127.6, 127.3, 127.3, 127.2, 126.7, 125.9, 125.9, 125.2, 125.2, 125.0, 124.9, 124.8, 124.7, 123.5, 116.4, 112.7, 77.2, 68.1, 33.6, 31.7, 29.2, 26.2. DEPT 90 (101 MHz, CDCl_3), δ [ppm]: 132.6, 127.9, 127.6, 127.6, 126.9, 126.2, 125.2, 125.2, 125.0, 123.8, 116.4. DEPT 135 (101 MHz, CDCl_3), δ [ppm]: 132.2, 127.6, 127.3, 127.2, 126.6, 125.9, 125.8, 124.9, 124.8, 124.7, 116.3, 68.1, 33.5, 31.6, 29.2, 26.2. FTIR (KBr), $[\text{cm}^{-1}]$: 3072, 2879, 1904, 1864, 1588, 1464, 1246, 1183, 997, 831, 743, 702, 625, 580, 490. HRMS (ESI): calcd $[m/z]$: 443.1005, found $[m/z]$: 442.1015.

2.2.1.4. Preparation of 4-((5-(pyrene-1-yl)pentyl)oxy)phenyl)boronic Acid (4). 5-(4-Bromophenoxy)pentylpyrene (3.00 g, 6.77 mmol) and anhydrous THF (50 mL) were added to a dry 100 mL round-bottom flask. After complete dissolution, the flask was cooled in an isopropanol/dry ice bath to -78 °C before $n\text{-BuLi}$ (2.97 mL of a 2.5 M solution in hexane, 7.44 mmol, 1.1 equiv) was added dropwise. The intense yellow color of the reaction mixture was observed during the addition of $n\text{-BuLi}$. The vessel's contents were vigorously stirred for 1 h at -78 °C, and then B(OMe) (7.54 mL, 67.66 mmol, 10.0 equiv) was added. The stirring of the solution was continued for another 2 h at -78 °C. The reaction was stopped by adding saturated NH_4Cl solution (5 mL). 4-((5-(pyrene-1-yl)pentyl)oxy)phenyl boronic acid was synthesized as a white solid (2.04 g, 74%). mp: 129.0–130.0 °C; R_f (AcOEt/hexane: 1:1, v/v) = 0.52; ^1H NMR (400 MHz, CDCl_3), δ [ppm]: 8.30 (d, $J = 9.2$ Hz, 1H), 8.21–7.81 (m, 9H), 6.99 (d, $J = 8.2$ Hz, 2H), 4.08 (t, $J = 6.3$ Hz, 2H), 3.41 (t, $J = 7.6$ Hz, 2H), 2.09–1.85 (m, 4H), 1.79–1.64 (m, 2H). ^{13}C NMR (101 MHz, CDCl_3), δ [ppm]: 163.1, 137.7, 137.0, 135.4, 131.8, 131.3, 130.1, 129.2, 129.0, 128.4, 127.7, 127.4, 126.8, 126.0, 125.5, 125.4, 125.0, 125.0, 124.9, 123.6, 114.4, 77.2, 68.1, 33.6, 31.7, 29.4, 26.4. DEPT 90 (101 MHz, CDCl_3), δ [ppm]: 137.7, 127.8, 127.4, 126.8, 126.0, 125.1, 125.0, 124.9, 123.6, 114.4. DEPT 135 (101 MHz, CDCl_3), δ [ppm]: 137.7, 137.7, 127.7, 127.4, 126.8, 126.0, 125.0, 124.9, 114.4, 114.4, 68.1, 33.64, 31.7, 29.5, 26.4. FTIR (KBr), $[\text{cm}^{-1}]$: 3423, 3243, 3033, 2928, 2858, 1594, 1504, 1466, 1414, 1350, 1245, 1169, 1038, 1000, 969, 923, 835, 748, 691, 587, 517. HRMS (ESI): calcd $[m/z]$: 407.1928, found $[m/z]$: 407.1946.

2.2.2. Procedure for the Synthesis of the Amidation Catalyst. CNO (0.200 g), 4-((5-(pyrene)pentyl-1-yl)oxy)phenyl boronic acid (0.476 g, 1.17 mmol), and toluene/ CHCl_3 : 4:1, v/v (30 mL) were added to a PP vial (50 mL). The resulting suspension was sonicated in an ultrasonic bath at 50 °C for 1 h and then stirred intensively for 12 h at RT. The carbon material was centrifuged using a rotary centrifuge (7800 rpm, 10 min), and the supernatant solution was

decanted. Toluene (50 mL) was added to the solid residue, and the resulting suspension was sonicated for 1 min at RT. The carbon material was centrifuged again, and the decanted liquid was discarded. Washing was performed identically three times (3×50 mL). Then, the washed carbon material was dried in a vacuum desiccator (20 mBa, RT, 12 h). Finally, the carbon catalyst (5) was obtained as a black powdery solid (0.403 g). FTIR (KBr), $[\text{cm}^{-1}]$: 3406, 2969, 2911, 2168, 1635, 1390, 1242, 1163, 1003, 1058, 886, 883, 508.

2.2.3. General Procedure A (P1) for the Synthesis of Amides via Aryl Boronic Acid 5-Catalyzed Amide Bond Formation. Carboxylic acid (2.0 mmol), amine (2.0 mmol), DMAPO hydrate (0.014 g, 0.101 mmol, 5 mol %), and carbon catalyst 5 (30 mg) were mixed in an agate mortar. Then, the solid was transferred to a 10 mL MW tube (1.2 cm ID), purged with Ar, and sealed with a cap. The tube was heated in the microwave (150 °C, 1 h, 200 W) and then cooled to 55 °C. The mixture was transferred, with hot toluene, into a vial adapted for an automatic centrifuge and made up to a total volume of 50 mL with solvent. The resulting suspension was sonicated at RT for 5 min, and then the catalyst was centrifuged, and the supernatant solution was decanted. The washing procedure was carried out two times with the mixture AcOEt/toluene: 2:8, v/v (2×20 mL). Catalyst 5 was left in the regeneration tube. The collected organic layers were washed in a separating funnel with 10% citric acid solution (2×20 mL), then with 20% K_2CO_3 solution (2×20 mL) and saturated NaCl solution (1×20 mL). The extracts were then dried with anhydrous Na_2SO_4 and filtered through a cotton tube, and the solvents were evaporated on a rotary evaporator under reduced pressure. The dry residue was purified by FCC chromatography on silica gel to yield the desired product.

The amide coupling reaction cannot take place in an environment in which copper(II) salts and oxygen are present due to the possibility of a competitive coupling reaction of aryl boronic acids (the structural part of the catalyst 4) with aromatic amines toward the formation of diarylamines. For this reason, the anaerobic conditions of the reaction were necessary.

2.2.4. General Procedure B (P2) for the Synthesis of Amides via Aryl Boronic Acid 4-Catalyzed Amide Bond Formation. Carboxylic acid (2.0 mmol), amine (2.0 mmol), DMAPO hydrate (0.014 g, 0.101 mmol, 5 mol %), and 4-((5-(pyrene-1-yl)pentyl)oxy)phenyl boronic acid (4) (0.041 g, 0.1 mmol, 5 mol %) were mixed using an agate mortar. The mixture was then transferred to a 10 mL MW tube (1.2 cm ID), purged with Ar, and sealed with a cap. The tube was heated under MW (150 °C, 1 h, 200 W) and then cooled to 55 °C. The reaction mixture was transferred with DCM (100 mL) to a separatory funnel. The organic layer was washed with a 10% citric acid solution (2×20 mL), a 20% K_2CO_3 solution (2×20 mL), and a saturated NaCl solution (1×20 mL). The extracts were then dried with anhydrous Na_2SO_4 and filtered through a cotton tube, and the solvent was removed by rotary evaporation under reduced pressure. The dry residue was purified by FCC chromatography on silica gel to yield the desired product.

2.2.5. General Procedure C (P3) for the Regeneration of the Carbon Catalyst 5. The contaminated carbon catalyst (5), separated from the reaction mixture, remained in the 50 mL tube and was washed with 10% AcOH solution (1×10 mL) and then with acetone/ H_2O : 1:1, v/v (2×30 mL). After each addition of the washing solution, the tube with the carbon material was sonicated at RT for 30 s, then the carbon material was centrifuged on a rotary centrifuge (7850 rpm, 10 min), and the supernatant solution was decanted. The purified catalyst was dried under reduced pressure in a vacuum desiccator (50 mBa, RT). Finally, the recovered catalyst can be used multiple times.

3. RESULTS AND DISCUSSION

3.1. Preparation of Nanostructured Carbon Catalyst and Its Characterization. The most common and economical method used to produce spherical CNO is the method proposed by Kuznetsov, which was further modified and applied by other authors.^{48,51,52} The nanostructures were

obtained in the thermal annealing process at high temperatures (1650 °C) from diamond nanoparticles in an inert gas atmosphere (Figure 1A,B). Commercially available NDs with

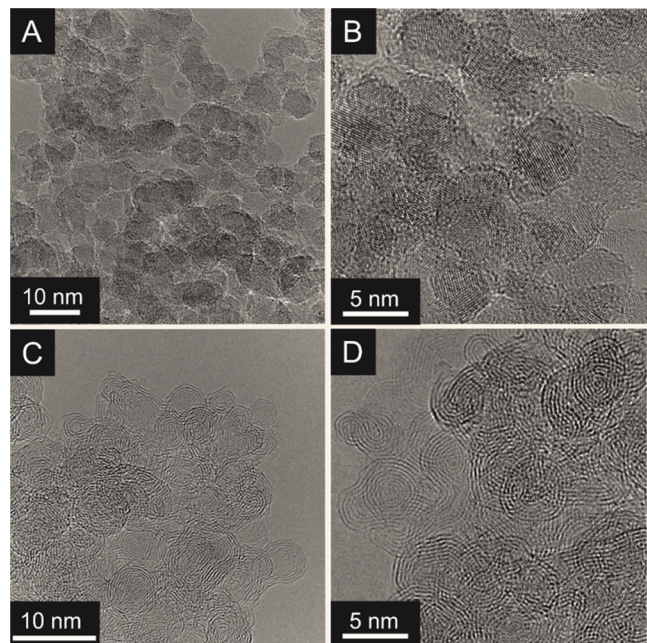


Figure 1. HRTEM images with the different magnifications of (A, B) nanodiamonds and (C, D) CNOs.

a crystal size between 4 and 6 nm were used to prepare CNOs. Under these conditions, the nanodiamond core is transformed into spherical multilayered structures. The formed carbon nanostructures have a cage-within-cage system, with smaller fullerenes nested inside larger ones (Figure 1C,D). The multiple layers of nested concentric graphitic shells are composed of 4–11 layered nanoparticles with a size of about 4–8 nm (Figure 1D). An intershell spacing estimated from the

high-resolution transmission electron microscopy (HRTEM) diffraction patterns is around 0.34 nm. The nanodiamond-derived CNO has greater surface curvature and strain energy, which leads to higher chemical reactivity than other larger carbon nanostructures. Therefore, a CNO was used as a carbon scaffold to immobilize the aryl boronic acid (4). As a result, we prepared a nanostructured carbon catalyst 5.

A heterogeneous nanostructured carbon catalyst (5) containing CNOs and aryl boronic acid (4) was synthesized (Figure 2). Aryl boronic acid (4) was initially synthesized in a four-step process starting from pyrene. In the first step, pyrene was brominated with *N*-bromosuccinimide (NBS) catalyzed with lauryl peroxide to give a 1-bromopyrene (1) yield of 87%.^{53,54} The bromine atom of compound 1 was lithiated with *n*-BuLi, and thus the generated nucleophilic intermediate was subjected to S_N2 substitution with 1,5-dibromopentane to give 1-(5-bromopentyl)pyrene (2) in 84% yield. High selectivity of the substitution reaction was achieved due to the excess of 1,5-dibromopentane used at the low temperature. The bromine atom of compound 2 was subjected to an S_N2 substitution reaction with sodium 4-bromophenolate.

The use of DMF as a reaction medium and MW heating allows the synthesis of 1-(5-(4-bromophenoxy)pentyl)pyrene (3) with a yield of 91%. Next, the bromine atom of compound 3 was subjected to a lithium substitution reaction, and the synthesized nucleophilic intermediate was sequentially reacted with an excess of trimethyl orthoborate, yielding (4-((5-(pyrene-1-yl)pentyl)oxy)phenyl)boronic acid (4) with the efficiency of 74%. Finally, an amide coupling catalyst (5) was prepared by π - π interaction of aryl boronic acid (4) and the CNO surface (Figure 3). A high degree of adsorption was achieved by sonication of the CNO dispersion and compound 4 in a mixture of toluene/CHCl₃ (4:1, v/v).

Fourier transform infrared spectroscopy (FTIR) was utilized to confirm the noncovalent immobilization of catalyst 4 on the CNO surface to form catalyst 5 (Figure 3). The pyrene moieties have several characteristics of absorption bands. The signal at 3040 cm⁻¹ corresponds to C–H stretching vibrations

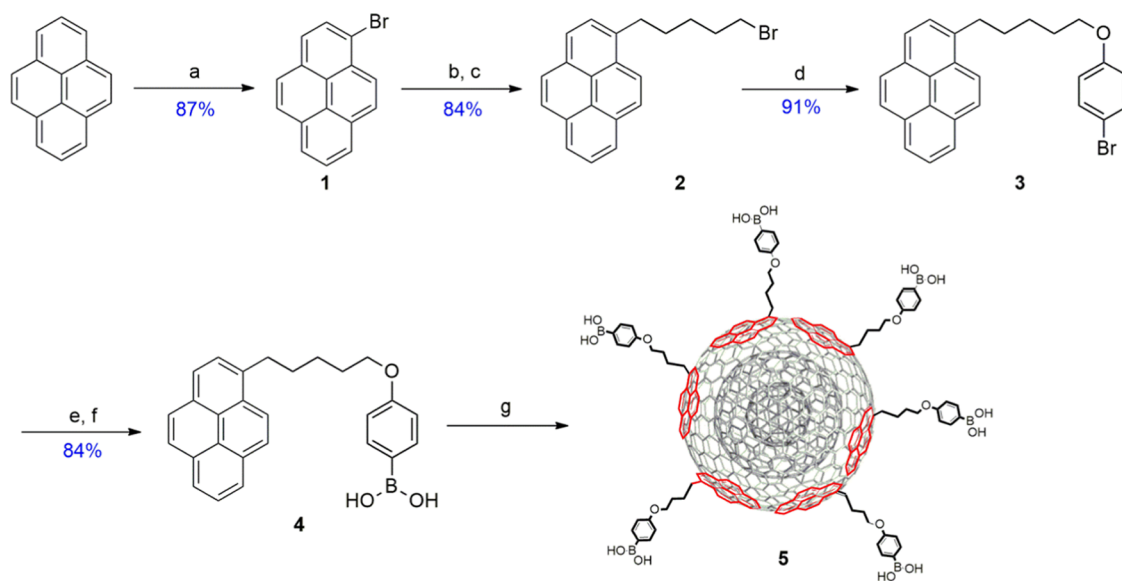


Figure 2. Preparation of the nanostructured carbon-catalyst (5). Reaction conditions: (a) NBS, lauryl peroxide, DMF, RT; (b) *n*-BuLi, -78 °C; (c) 1,5-dibromopentane, THF, -78 and 0 °C, NH₄Cl; (d) 4-bromophenol, NaOH, DMF, MW; (e) *n*-BuLi, THF, -78 °C; (f) B(OMe)₃, -78 °C, NH₄Cl; and (g) CNOs, toluene/CHCl₃ (4:1, v/v), RT.

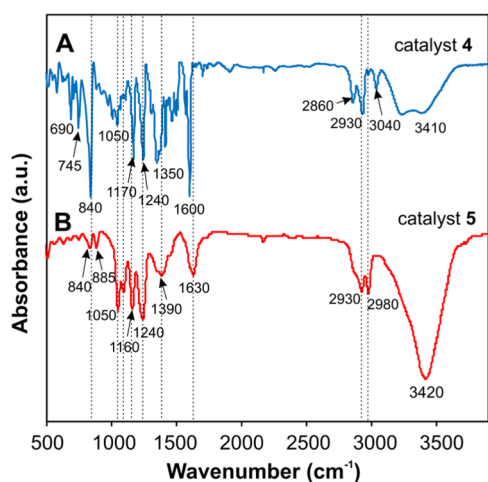


Figure 3. FTIR spectra of catalysts (A) 4 and (B) 5.

of sp^2 -hybridized carbon atoms (Figure 3A).^{55,56} The peaks at 2930 and 2830 cm^{-1} can be assigned to asymmetric and symmetric stretching vibrations corresponding to the sp^3 -hybridized carbon atoms. Next, the peak in the range of 1630–1600 cm^{-1} is correlated with the conjugated carbons ($-C=C-$, stretching vibrations) in the pyrene moieties (Figure 3A,B). In the lower wavenumber values, at 745 and 690 cm^{-1} , the CH_2 wagging vibrations were detected (Figure 3A).^{56,57} The remaining signals related to the absorption of IR radiation confirm the presence of boric acid in the structure of catalysts 4 and 5 (Figure 3). The broad signals in the higher frequency range (3500–3600 cm^{-1}) correspond to $-O-H$ stretching vibrations (Figure 3).

The four strong signals located between 1400 and 1150 cm^{-1} , with the maximum at 1390, 1350, 1240, and 1170 cm^{-1} , are caused by asymmetric B–O stretching and in-plane B–O–H bending.⁵⁸ Additionally, absorption at 840 cm^{-1} can be assigned to symmetric B–O stretching or out of plane B–O–H bending.⁵⁸ These peaks with lower intensities are also present in the spectra for catalyst 5 (Figure 3B).

Scanning electron microscopy (SEM) with the energy dispersive X-ray (EDX) analysis was performed to study the morphology and elemental composition of the synthesized nanostructured materials (Figure S71). The SEM images of a gold foil covered with CNO are shown in Figure S71A,B. The CNO formed large aggregates of the nanoparticles, even more, significant than 100 μm , with a heterogeneous distribution. The morphology of the nanostructured catalyst 5 exhibits porous structures with many channels and outcroppings (Figure S71C). It is due to the formation of agglomerates with sizes smaller than 20 μm . The EDX analysis of catalyst 5 reveals that the material contains C, B, and O with 86, 2, and 0%, respectively (Figures S71D–H). The distribution of elements in the nanostructured material is homogeneous.

The high thermal stability of catalysts is one of the most important parameters required for effective organic catalysis. The thermal stability and decomposition of the catalysts were performed using thermogravimetric (TG) analysis. The TG and derivative thermogravimetric (DTG) curves of the studied materials are presented in Figure 4. The decomposition range and percentage of weight loss are summarized in Table 1. Decomposition of the catalysts in an Ar or an O_2 atmosphere suggests different mechanisms of these processes. The studies in an Ar atmosphere show the decomposition of the organic

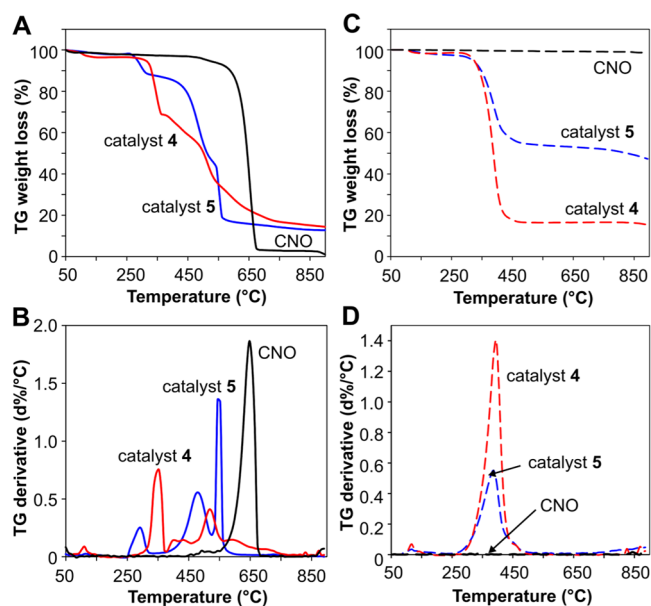


Figure 4. (A, C) Thermo-gravimetric analysis (TGA) and (B, D) DTG results of catalyst 4 (red line), nonmodified CNO (black line), and catalytic nanostructured carbon-material (5) (blue line) under an O_2 (left) and Ar atmosphere (right).

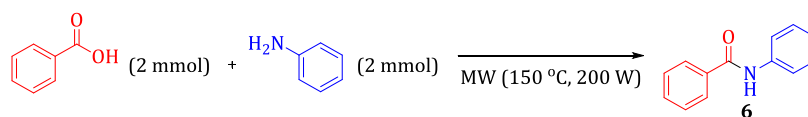
part while maintaining the CNO, which did not decompose up to 900 $^{\circ}C$.

The multilayered structure ensures high thermal stability. Combustion in an O_2 atmosphere leads to the oxidation of not only catalyst 4 but also the nanostructured carbon catalyst. The catalyst 4 adsorbed on the CNO surface is more thermally stable than the pure catalyst 4. The inorganic residue of boron oxide after the combustion process is 18 or 13%, respectively, for catalysts 4 and 5. The analysis under these conditions also shows the amount of aryl boronic acid (catalyst 4) adsorbed on the surface of the nanostructural carbon (CNO), which is about 35% by weight of catalyst 5, respectively (Figure 4 and Table S1).

CNOs as a component of the catalyst 5 are oxidized at the lower temperature and in a narrower temperature range (532–562 $^{\circ}C$) compared to nonmodified carbon nanostructures (561–682 $^{\circ}C$), which is the result of an influence of the pyrene moieties on the thermal stability of CNO (Figure 4). However, the use of CNO as a carbon matrix for the immobilization of pyrene moieties causes a significant increase in the thermal stability of catalyst 5 compared to catalyst 4.

3.2. Optimization of the Catalytic Reaction Condition. We selected a model direct amidation reaction of benzoic acid and aniline catalyzed by aryl boronic acid (4) or the nanostructured carbon catalyst (5) to screen the different reaction parameters (Table 1). All reactions were performed under a MW heating condition. No reaction occurred in the control experiment without catalysts (4 or 5) and with the addition of solvent, even if molecular sieves were used as a dehydrating reagent (entries 1–3). It was determined that the maximum reaction efficiency without a catalyst under solvent-free conditions was 12% (entry 4). As a control reaction, we also performed the amide coupling reaction with CNO (entries 5 and 6). The reaction was carried out with a low efficiency of about 24% using a relatively long time of 240 min.

Adding catalyst 4 to the reaction medium did not improve the reaction yield (14%, entry 7, Table 1), which results from

Table 1. Optimization of the Reaction Conditions^a

entry	catalyst	amount of catalyst	additive	amount of additive	solvent	time (min)	yield (%) ^a
1			MS 3 Å	0.25 g mmol ⁻¹	toluene	30	
2			MS 3 Å	0.25 g mmol ⁻¹	toluene	120	
3			MgSO ₄	0.25 g mmol ⁻¹	toluene	30	
4						30	12
5	CNO	15 mg mmol ⁻¹				30	17
6	CNO	15 mg mmol ⁻¹				240	24
7	4	5 mol %	MS 3 Å	0.25 g mmol ⁻¹	toluene	120	14
8	4	5 mol %	MgSO ₄	0.25 g mmol ⁻¹		30	10
9	4	5 mol %				30	23
10	4	10 mol %				60	38
11	5	15 mg mmol ⁻¹			toluene	30	11
12	5	15 mg mmol ⁻¹				30	42
13	5	15 mg mmol ⁻¹	imidazole	5 mol %		30	51
14	5	15 mg mmol ⁻¹	Et ₃ N	5 mol %		30	43
15	5	15 mg mmol ⁻¹	NHS	5 mol %		30	47
16	5	15 mg mmol ⁻¹	DMAP	5 mol %		30	48
17	5	15 mg mmol ⁻¹	DMAPO·H ₂ O	5 mol %		45	79
18	5	15 mg mmol ⁻¹	DMAPO·H ₂ O	5 mol %		60	88
19	5	15 mg mmol ⁻¹	DMAPO·H ₂ O	5 mol %		90	87
20	5	15 mg mmol ⁻¹	DMAPO·H ₂ O	10 mol %		60	88
21	5	15 mg mmol ⁻¹	DMAPO·H ₂ O	15 mol %		60	89
22	5	15 mg mmol ⁻¹	DMAPO·H ₂ O	20 mol %		60	88
23	5	15 mg mmol ⁻¹	DMAPO·H ₂ O	30 mol %		60	85
24	5	15 mg mmol ⁻¹	DMAPO·H ₂ O	100 mol %		60	73
25	4	5 mol %	DMAPO·H ₂ O	5 mol %		60	52
26	4	5 mol %	DMAPO·H ₂ O	10 mol %		60	55
27			DMAPO·H ₂ O	5 mol %		60	15
28			DMAPO·H ₂ O	5 mol %		240	21
29			DMAPO·H ₂ O	10 mol %		60	20
30			DMAPO·H ₂ O	15 mol %		60	19

^aIsolated yield of pure product. Molecular sieves 3 Å (MS 3 Å); triethylamine (Et₃N); *N*-hydroxysuccinimide (NHS); 4-(dimethylaminino)pyridine (DMAP); and 4-(*N,N*-dimethylamino)pyridine *N*-oxide hydrate (DMAPO·H₂O).

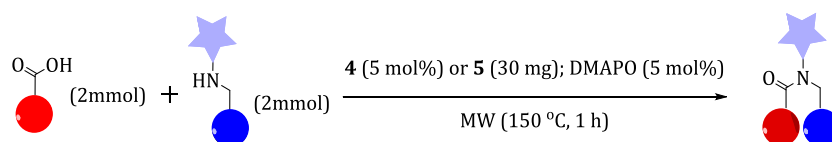
the thermal effect if the reaction was carried out in solution in the interval. Moreover, conducting the reaction under solvent-free conditions and in the presence of MgSO₄ as a dehydrating reagent did not increase the yield (entry 8). It prevented liquefaction of the mixture of the reagents (entry 8). When amine and acid (1:1 molar ratio) were ground in a mortar and heated under MW at 150 °C, the reaction proceeded with a 23% yield (entry 9). Doubling the concentration of catalyst 4 and the reaction time slightly increases the reaction efficiency to 38% (entry 10).

The direct amide coupling reaction with the nanostructured carbon catalyst (5) was carried out similarly under the MW-assisted solvent-free conditions (entry 12, Table 1) or with solvent addition (entry 11). The presence of an additional catalyst structural component, i.e., CNO, caused the reaction under conditions without adding a solution to increase the yield of the reaction fourfold, from 11 to 42% (entries 11 and 12). Moreover, we found that adding organic bases (Et₃N, DMAP, or imidazole) to the reaction improved the yield from 42 to 43, 48, and 51%, respectively (entries 14, 16, and 13). We also improved reaction yield by up to 47% with the addition of *N*-hydroxysuccinimide (NHS) (entry 15). As it turned out, 4-(*N,N*-dimethylamino)pyridine *N*-oxide

(DMAPO) was the most effective promoter of our model reaction for all used additives.

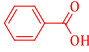
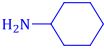
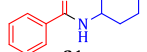
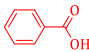
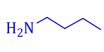
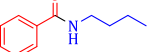
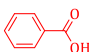
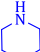
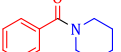
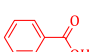

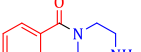
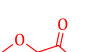
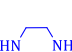
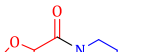
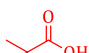
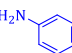
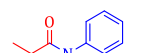



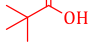
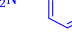
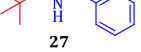
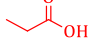
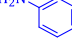
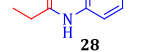
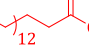
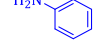
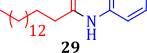
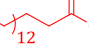
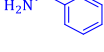
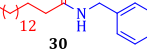
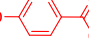
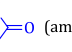
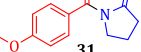
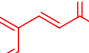
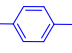
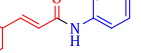
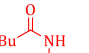
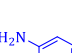
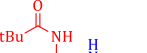
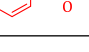

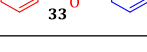

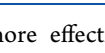
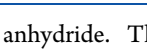
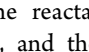
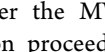
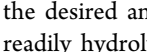
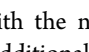
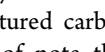
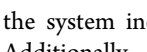
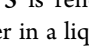
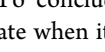
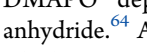
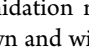
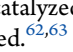
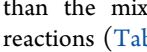
We investigated the effect of DMAPO additive due to previous literature reports of its ability to promote amide coupling reactions catalyzed by aryl boronic acid under solvent-free conditions and the influence of MW heating.^{59–61} Time screening showed that 60 min was sufficient for the reaction. Therefore, we determined the optimal conditions described in entry 18, which allowed us to obtain the amide at the yield level of 88%. Further increase in the reaction time does not affect the efficiency of the catalytic reaction (entry 19). We also examined the effect of DMAPO concentration ranging from 5 to 100 mol % on the performance of the direct amide coupling reaction (entries 18 and 20–24). The reaction efficiency does not change in the studied concentration range. However, it should be noted that the reaction yield decreased for the highest DMAPO concentration (100 mol %, entry 24). We also performed the amide coupling reaction with DMAPO with catalyst 4 (entries 25 and 26). The reaction ran with a lower efficiency of about 55%. The reaction without the addition of catalysts 4 or 5 also proceeds with a meager yield in the presence of DMAPO. Within 240 min, the reaction product is obtained with a yield of about 21% (entry 28).

Table 2. Scope of the Amidation Reaction Catalyzed by 4 or 5



Entry	Carboxylic Acid	Amine	Product	Catalyst	Isolated Yield (%) ^a
1				4	79
2				5	80
3				4	82
4				5	93
5				4	39
6				5	47
7				4	46
8				5	53
9				4	89
10				5	94
11				4	78
12				5	80
13				4	60
14				5	69
15				4	92
16				5	93
17				4	74
18				5	76
19				4	88
20				5	92
21				4	80
22				5	89
23				4	85
24				5	91
25				4	90
26				5	95
27				5	27

Table 2. continued

Entry	Carboxylic Acid	Amine	Product	Catalyst	Isolated Yield (%) ^a
28				4	83
29				5	87
30				5	52
31				5	67
32				5	77
33				4	82
34				5	87
35				4	82
36				5	88
37				4	89
38				5	96
39				4	87
40				5	92
41				4	85
42				5	90
43				4	90
44				5	97
45				5	No reaction
46				5	No reaction
47				5	No reaction

^aIsolated yield of the pure product.

The nanostructured carbon catalyst (**5**) is more effective than the aryl boronic acid (**4**) because the graphite structure ensures effective heating of the reactants under the MW-assisted solvent-free conditions, and the reaction proceeded homogeneously. It did not proceed efficiently when the reagents were not grounded with the nanostructured carbon catalyst before the reaction. Additionally, it is of note that nanostructured carbon catalyst **5** is renewable. To conclude, the yield of the reaction is higher in a liquefied state when it is homogeneously powdered with the carbon catalyst.

The mechanism of direct amidation reactions catalyzed by organic boron acids is well known and widely studied.^{62,63} Aryl boronic acids can polycondensate into aggregates and react with the carboxylic acids, resulting in a specifically mixed

anhydride. The nucleophilic attack of the amine on the carbonyl center of this species may involve the formation of the desired amide bond. Anhydride and aryl boronic acid are readily hydrolyzed in an aqueous medium. An equilibrium of the reaction is shifted toward forming an amide product when the system includes a factor reducing the amount of water.³ Additionally, it is postulated that the cocatalytic effect of DMAPO depends on interaction with the synthesized anhydride.⁶⁴ As a result, an active ester of DMAPO is formed, which reacts much more effectively with the aromatic amines than the mixed anhydride itself. Based on the conducted reactions (Table 1), we proposed the amide coupling reaction mechanism fulfilled in our experimental conditions (Figure S72, please see the Supporting Information). The aryl boronic

acid forms a mixed anhydride with the carboxylic acid (1st activation). An amide bond can be formed by the nucleophilic substitution of an amine for the electrophilic center of the anhydride. The presence of a nucleophilic cocatalyst for the reaction in the DMAPO mixture can, in the same substitution, lead to the formation of a salt of the DMAPO ester and aryl boronic acid (2nd activation). The present ester is also active in the nucleophilic substitution of the amine. The substituted tetrahedral intermediate state decomposes into an amide, reconstituting the salt of DMAPO and aryl boronic acid.

Next, we investigated the limitations of reactions involving various acids and bases catalyzed by **5** (Table 2). The conditions from entry 18 (Table 1) were used in all cases. For several amides (compounds **7–12**, **14**, and **16**, Table 2), we performed additional experiments consisting in converting the catalyst **5–4** to check whether there were discrepancies in the obtained yield. For both catalysts, the obtained results were similar, although slightly higher for those using nanostructured carbon catalyst **5**. It is of note that the synthesis and use of compound **4** have no practical value due to its lack of renewability than catalyst **5**. Therefore, further experiments were performed only with the target catalyst. The amidation reaction is generally more efficient with benzylamines than with the aniline derivatives. Additionally, the obtained yields are higher for the aniline derivatives with electro-donating substituents in the benzene ring (compounds **7** and **8**) than for electro-accepting ones (compounds **9** and **10**). The differences are probably due to the different basicity of these amines, which significantly change with the type of substitution on the benzene ring. The higher yields for the more basic benzylamine also support this theory. There is no relationship between the basicity of nonaromatic amine and the obtained yield of the synthesized amide (compounds **18–21**). The low yield of the synthesized compound **17** may be due to the high volatility of *N,N*-diethylamine, which hinders a homogenous course of the reaction in a MW vial. The amidation reaction was carried out for aliphatic acids (Table 2, entries 35–44). The reaction with aliphatic acids is generally more efficient than with aromatic acids. The reason may be the higher acidity (lower pK_a) of aliphatic acids than of aromatic acids and also often lower steric hindrance of the aliphatic substituent.

Although the nanostructured carbon catalyst (**5**) does not catalyze some of the reactions (compounds **31–33**, entries 45–47, Table 2), we have intentionally included the results, noting which compounds do not react in these experimental conditions. We checked that the reaction between the amide (2-pyrrolidone) and *p*-methoxy benzoic acid did not lead to the formation of an aniracetam drug (compound **31**). The reaction mixture did not liquefy during the reaction between *p*-nitroaniline and cinnamic acid, and therefore the amide **32** was not synthesized. Compound **33** was not synthesized due to the decomposition of the corresponding carboxylic acid under the reaction conditions.

3.3. Catalytic Activity of Nanostructured Carbon-Catalyst and Comparison with Other Catalysts. To assess the stability and the reusability of catalyst **5**, the model amide coupling reaction was performed in five successive runs (Figure 5). In the case of the nanostructured heterogeneous catalysts, the problems that are often emphasized at this scale of materials are their homogeneous dispersion in solution, mass-transfer limitations, and reusability.⁴⁷ The first two parameters in the reaction under MW heating are largely eliminated. In addition, using the solid-state conditions and CNO as an MW

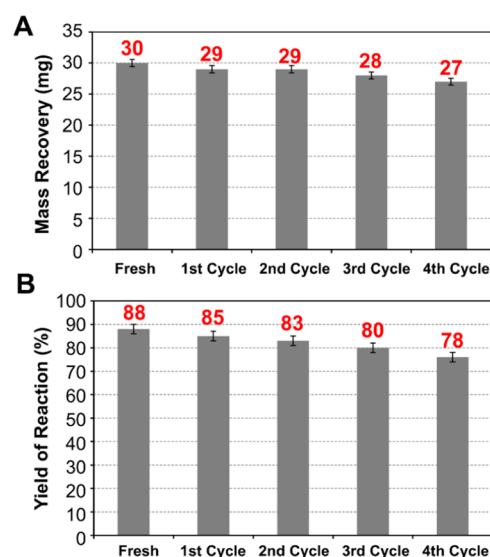


Figure 5. Reusability of catalyst **5**. (A) Mass recovery of catalyst **5** in the first five cycles. (B) Yield of the amide coupling reaction between benzoic acid and aniline catalyzed by materials **5** in the first five cycles.

absorber removes the problem of homogeneous dispersion of carbon nanostructures in the solution and mass-transfer limitations. The absorption of MW radiation by the CNO effectively influences the yield of the catalytic reaction. Additionally, the recovery of catalytic material is straightforward, and the mass losses are negligible. After five cycles, the reusability of catalyst **5** is at the level of 91% by mass (Figure 5A).

A comparison with other organic and inorganic catalytic systems in the direct amide coupling reaction demonstrated that our nanostructural carbon catalyst exhibited a high conversion and yield in a short reaction time (Table 3). By analyzing the data in the table, we can draw several conclusions. First, the amidation reaction for the aniline derivatives is more challenging (entries 1–5).

In the literature, we find only a few reports with this substrate, for which a much lower reaction yield is achieved than for our nanostructured carbon catalyst (88%, aniline derivatives, entry 6) (Table 3). Additionally, the reactions usually require organic solvents that are not environmentally friendly (entries 1 and 3–5). All of the reactions presented require the presence of a catalyst which requires additional removal from the reaction mixture due to the inorganic nature, which is considered to be an impurity of the product. The amidation reaction is generally more efficient with benzylamine (entries 7–18) than with the aniline derivatives. Reaching high yields of the amidation reaction is possible, even 98%, when using a long reaction time (between 3 and 24 h) and organic solvents. Shortening the time requires high-energy radiation, such as MW and RF (entries 13, 14, and 16). For the amidation reaction with benzylamine and catalyst **5**, we achieved 94% yield quickly (1 h, entry 18).

This short comparison with other literature examples clearly shows that using a modified nanostructured carbon-catalyst for the direct amide coupling reaction supported by MW radiation is a very effective method. It allows the elimination of organic solvents from the reaction environment and minimizes energy consumption, which consequently makes this catalytic method more environmentally friendly.

Table 3. Comparative Study of Catalysts

entry	catalyst	conditions	time (h)	yield (%)	refs
1	boric acid/PS supported	toluene ^a	40	50	22
2	CAN	MW (160 °C)	2	69–71	18
3	Kieselgel 60	toluene ^a	24	36	65
4	Kieselgel 60	<i>p</i> -cymene ^a	24	69	65
5	Nb ₂ O ₅	toluene ^a	30	80	66
6	catalyst 5	MW/DMAPO ^{c,d}	1	88	this work
7	boric acid/MCF	<i>o</i> -xylene ^a	5	83	23
8	B-Py salt	<i>o</i> -xylene-[emin][OTf] ^d	6	98	24
9	B(Ph) ₃	toluene ^b	3	9	67
10	B(OH) ₃	TAME ^a	24	20	68
11	B(OCH ₂ CF ₃) ₃			80	
12	B(OMe) ₃			45	
13	TiO ₂	MW	0.2	99	69
14	Fe ₂ H ₂ NiO ₄	RF heating	0.15	94	70
15	ZrCl ₄	THF	24	84	71
16	CAN	MW (160 °C)	2	71–77	18
17	Zr-AzoBDC	THF	24	66	72
18	catalyst 5	MW/DMAPO ^{c,e}	1	94	this work

^aAzeotropic removal of water. ^bReflux. ^cAt 150 °C (200 W). ^dAniline derivatives. ^eBenzylamine derivatives. PS: polystyrene; CAN: ceric ammonium nitrate; B-Py salt: alkyl-4-boronopyridinium salts; B(Ph)₃: triphenyl borate; TAME: *tert*-amyl methyl ether; RF: radiofrequency heating; and Zr-AzoBDC: azobenzene-containing metal–organic framework.

4. CONCLUSIONS

In conclusion, we have synthesized a very efficient heterogeneous nanostructured carbon catalyst for the direct amide coupling reaction using MW-heating in the absence of a solvent. Using a nanostructured carbon with adsorbed aryl boronic acid increases the thermal stability of the catalyst and its reusability. Additionally, using an MW-assisted synthesis in a solid-state condition eliminates the problem associated with the dispersion of the nanostructured carbon materials in solution and mass-transfer limitations. The absorption of MW radiation by the nanostructural catalyst effectively influences yield of the catalytic reaction, which is up to 94%. Additionally, the recovery of catalytic material is straightforward, and the mass losses are negligible. After five cycles, the reusability of catalyst 5 is at the level of 91% by mass. Usage of an effective nanostructural carbon MW absorber significantly affects the efficiency of the catalytic reaction and decreases the power consumption. Additionally, eliminating solvents from the catalytic reaction reduces the process costs and makes the reaction condition more environmentally friendly.

■ ASSOCIATED CONTENT

Supporting Information

The Supporting Information is available free of charge at <https://pubs.acs.org/doi/10.1021/acsnm.2c03437>.

Materials and methods; procedures for the synthesis of aryl boronic acid; characteristics of the synthesized amides; and spectral data for compounds (¹H, ¹³C NMR, and FTIR) (PDF)

■ AUTHOR INFORMATION

Corresponding Author

Marta E. Plonska-Brzezinska – Department of Organic Chemistry, Faculty of Pharmacy with the Division of Laboratory Medicine, Medical University of Białystok, 15-222 Białystok, Poland; orcid.org/0000-0002-0538-6059; Email: marta.plonska-brzezinska@umb.edu.pl

Authors

Damian Pawelski – Department of Organic Chemistry, Faculty of Pharmacy with the Division of Laboratory Medicine, Medical University of Białystok, 15-222 Białystok, Poland

Olivia Fernandez Delgado – University of Texas at El Paso, El Paso, Texas 79968-8807, United States; orcid.org/0000-0002-6641-026X

Agnieszka Z. Wilczewska – Faculty of Chemistry, University of Białystok, 15-245 Białystok, Poland; orcid.org/0000-0001-8587-6711

Jakub W. Strawa – Department of Pharmacognosy, Faculty of Pharmacy with the Division of Laboratory Medicine, Medical University of Białystok, 15-230 Białystok, Poland

Complete contact information is available at: <https://pubs.acs.org/doi/10.1021/acsnm.2c03437>

Notes

The authors declare no competing financial interest.

■ ACKNOWLEDGMENTS

The authors gratefully acknowledge the financial support of the National Science Centre, Poland, Grant #2019/35/B/ST5/00572 to M.E.P.-B. The authors gratefully acknowledge Prof. Luis Echegoyen from the University of Texas at El Paso for providing the CNOs. We gratefully acknowledge Dr. Habil Michal Tomczyk (Medical University of Białystok) for the possibility of performing HRMS measurements. We also thank Dr. Joanna Breczko (University of Białystok) for performing SEM with EDX measurements.

■ REFERENCES

- Valeur, E.; Bradley, M. Amide Bond Formation: Beyond the Myth of Coupling Reagents. *Chem. Soc. Rev.* **2009**, *38*, 606–631.
- Ghose, A. K.; Viswanadhan, V. N.; Wendoloski, J. J. A Knowledge-Based Approach in Designing Combinatorial or Medicinal Chemistry Libraries for Drug Discovery. 1. A Qualitative and Quantitative Characterization of Known Drug Databases. *J. Comb. Chem.* **1999**, *1*, 55–68.
- Charville, H.; Jackson, D.; Hodges, G.; Whiting, A. The Thermal and Boron-Catalysed Direct Amide Formation Reactions: Mechanistically Understudied yet Important Processes. *Chem. Commun.* **2010**, *46*, 1813–1823.
- Jursic, B. S.; Zdravkovski, Z. A Simple Preparation of Amides from Acids and Amines by Heating of Their Mixture. *Synth. Commun.* **1993**, *23*, 2761–2770.
- Wang, S.-M.; Zhao, C.; Zhang, X.; Qin, H.-L. Clickable Coupling of Carboxylic Acids and Amines at Room Temperature Mediated by SO₂F₂: A Significant Breakthrough for the Construction of Amides and Peptide Linkages. *Org. Biomol. Chem.* **2019**, *17*, 4087–4101.
- Liu, J.; Wang, S.-M.; Qin, H.-L. Room Temperature Clickable Coupling Electron Deficient Amines with Sterically Hindered Carboxylic Acids for the Construction of Amides. *Tetrahedron* **2020**, *76*, No. 131724.
- Wang, S.-P.; Cheung, C. W.; Ma, J.-A. Direct Amidation of Carboxylic Acids with Nitroarenes. *J. Org. Chem.* **2019**, *84*, 13922–13934.

- (8) Coomber, C. E.; Laserna, V.; Martin, L. T.; Smith, P. D.; Hailes, H. C.; Porter, M. J.; Sheppard, T. D. Catalytic Direct Amidations in *Tert*-Butyl Acetate Using B(OCH₂CF₃)₃. *Org. Biomol. Chem.* **2019**, *17*, 6465–6469.
- (9) Gelens, E.; Smeets, L.; Sliedregt, L. A. J. M.; van Steen, B. J.; Kruse, C. G.; Leurs, R.; Orru, R. V. A. An Atom Efficient and Solvent-Free Synthesis of Structurally Diverse Amides Using Microwaves. *Tetrahedron Lett.* **2005**, *46*, 3751–3754.
- (10) Wang, X.; Yang, Q.; Liu, F.; You, Q. Microwave-Assisted Synthesis of Amide under Solvent-free Conditions. *Synth. Commun.* **2008**, *38*, 1028–1035.
- (11) Menéndez, J.; Arenillas, A.; Fidalgo, B.; Fernández, Y.; Zubizarreta, L.; Calvo, E. G.; Bermúdez, J. M. Microwave Heating Processes Involving Carbon Materials. *Fuel Process. Technol.* **2010**, *91*, 1–8.
- (12) Perreux, L.; Loupy, A.; Volatron, F. Solvent-Free Preparation of Amides from Acids and Primary Amines under Microwave Irradiation. *Tetrahedron* **2002**, *58*, 2155–2162.
- (13) Tang, P. Boric Acid Catalyzed Amide Formation from Carboxylic Acids and Amines: N-Benzyl-4-phenylbutyramide: (Benzenebutanamide, N-(Phenylmethyl)-). In *Organic Syntheses*; John Wiley & Sons, Inc.: Hoboken, NJ, USA, 2005; pp 262–272.
- (14) Du, Y.; Barber, T.; Lim, S. E.; Rzepa, H. S.; Baxendale, I. R.; Whiting, A. A Solid-Supported Arylboronic Acid Catalyst for Direct Amidation. *Chem. Commun.* **2019**, *55*, 2916–2919.
- (15) Ishihara, K.; Ohara, S.; Yamamoto, H. (3,4,5-trifluorophenyl)-boronic acid-catalyzed amide formation from carboxylic acids and amines: n-benzyl-4-phenylbutyramide. *Org. Synth.* **2002**, *79*, No. 176.
- (16) Yamashita, R.; Sakakura, A.; Ishihara, K. Primary Alkylboronic Acids as Highly Active Catalysts for the Dehydrative Amide Condensation of α -Hydroxycarboxylic Acids. *Org. Lett.* **2013**, *15*, 3654–3657.
- (17) Chandra Shekhar, A.; Ravi Kumar, A.; Sathaiiah, G.; Luke Paul, V.; Sridhar, M.; Shanthan Rao, P. Facile N-Formylation of Amines Using Lewis Acids as Novel Catalysts. *Tetrahedron Lett.* **2009**, *50*, 7099–7101.
- (18) Zarecki, A. P.; Kolanowski, J. L.; Markiewicz, W. T. Microwave-Assisted Catalytic Method for a Green Synthesis of Amides Directly from Amines and Carboxylic Acids. *Molecules* **2020**, *25*, No. 1761.
- (19) Li, Z.; Liu, L.; Xu, K.; Huang, T.; Li, X.; Song, B.; Chen, T. Palladium-Catalyzed N-Acylation of Tertiary Amines by Carboxylic Acids: A Method for the Synthesis of Amides. *Org. Lett.* **2020**, *22*, 5517–5521.
- (20) Bongers, J.; Heimer, E. P. Recent Applications of Enzymatic Peptide Synthesis. *Peptides* **1994**, *15*, 183–193.
- (21) Lundberg, H.; Tinnis, F.; Selander, N.; Adolfsson, H. Catalytic Amide Formation from Non-Activated Carboxylic Acids and Amines. *Chem. Soc. Rev.* **2014**, *43*, 2714–2742.
- (22) Latta, R.; Springsteen, G.; Wang, B. Development and Synthesis of an Arylboronic Acid-Based Solid-Phase Amidation Catalyst. *Synthesis* **2001**, *2001*, 1611–1613.
- (23) Gu, L.; Lim, J.; Cheong, J. L.; Lee, S. S. MCF-Supported Boronic Acids as Efficient Catalysts for Direct Amide Condensation of Carboxylic Acids and Amines. *Chem. Commun.* **2014**, *50*, 7017–7019.
- (24) Maki, T.; Ishihara, K.; Yamamoto, H. N-Alkyl-4-Boronopyridinium Salts as Thermally Stable and Reusable Amide Condensation Catalysts. *Org. Lett.* **2005**, *7*, 5043–5046.
- (25) Ishihara, K.; Kondo, S.; Yamamoto, H. 3,5-Bis(Perfluorodecyl)-Phenylboronic Acid as an Easily Recyclable Direct Amide Condensation Catalyst. *Synlett* **2001**, *2001*, 1371–1374.
- (26) Yu, D.; Nagelli, E.; Du, F.; Dai, L. Metal-Free Carbon Nanomaterials Become More Active than Metal Catalysts and Last Longer. *J. Phys. Chem. Lett.* **2010**, *1*, 2165–2173.
- (27) Chen, R. J.; Zhang, Y.; Wang, D.; Dai, H. Noncovalent Sidewall Functionalization of Single-Walled Carbon Nanotubes for Protein Immobilization. *J. Am. Chem. Soc.* **2001**, *123*, 3838–3839.
- (28) Franco, J. H.; Klunder, K. J.; Lee, J.; Russell, V.; de Andrade, A. R.; Minter, S. D. Enhanced Electrochemical Oxidation of Ethanol Using a Hybrid Catalyst Cascade Architecture Containing Pyrene-TEMPO, Oxalate Decarboxylase and Carboxylated Multi-Walled Carbon Nanotube. *Biosens. Bioelectron.* **2020**, *154*, No. 112077.
- (29) Taher, A.; Lee, K. C.; Han, H. J.; Kim, D. W. Pyrene-Tagged Ionic Liquids: Separable Organic Catalysts for S_N2 Fluorination. *Org. Lett.* **2017**, *19*, 3342–3345.
- (30) Reuillard, B.; Ly, K. H.; Rosser, T. E.; Kuehnel, M. F.; Zebger, I.; Reisner, E. Tuning Product Selectivity for Aqueous CO₂ Reduction with a Mn(Bipyridine)-Pyrene Catalyst Immobilized on a Carbon Nanotube Electrode. *J. Am. Chem. Soc.* **2017**, *139*, 14425–14435.
- (31) Zhang, X.; Wang, B.; Lu, Y.; Xia, C.; Liu, J. Homogeneous and Noncovalent Immobilization of NHC-Cu Catalyzed Azide-Alkyne Cycloaddition Reaction. *Mol. Catal.* **2021**, *504*, No. 111452.
- (32) Maurin, A.; Robert, M. Noncovalent Immobilization of a Molecular Iron-Based Electrocatalyst on Carbon Electrodes for Selective, Efficient CO₂-to-CO Conversion in Water. *J. Am. Chem. Soc.* **2016**, *138*, 2492–2495.
- (33) Wittmann, S.; Schätz, A.; Grass, R. N.; Stark, W. J.; Reiser, O. A Recyclable Nanoparticle-Supported Palladium Catalyst for the Hydroxycarbonylation of Aryl Halides in Water. *Angew. Chem., Int. Ed.* **2010**, *49*, 1867–1870.
- (34) Qiu, L.-Q.; Chen, K.-H.; Yang, Z.-W.; He, L.-N. A Rhenium Catalyst with Bifunctional Pyrene Groups Boosts Natural Light-Driven CO₂ Reduction. *Green Chem.* **2020**, *22*, 8614–8622.
- (35) Plonska-Brzezinska, M. E. Carbon Nano-Onions: A Review of Recent Progress in Synthesis and Applications. *ChemNanoMat* **2019**, *5*, 568–580.
- (36) Bartkowski, M.; Giordani, S. Supramolecular Chemistry of Carbon Nano-Onions. *Nanoscale* **2020**, *12*, 9352–9358.
- (37) Kuzhir, P.; Maksimenko, S.; Bychanok, D.; Kuznetsov, V.; Moseenkov, S.; Mazov, I.; Shenderova, O.; Lambin, Ph. Nano-Scaled Onion-like Carbon: Prospective Material for Microwave Coatings. *Metamaterials* **2009**, *3*, 148–156.
- (38) Zeiger, M.; Jäckel, N.; Mochalin, V. N.; Presser, V. Review: Carbon Onions for Electrochemical Energy Storage. *J. Mater. Chem. A* **2016**, *4*, 3172–3196.
- (39) Grądzka, E.; Winkler, K.; Borowska, M.; Plonska-Brzezinska, M. E.; Echegoyen, L. Comparison of the Electrochemical Properties of Thin Films of MWCNTs/C60-Pd, SWCNTs/C60-Pd and Ox-CNOs/C60-Pd. *Electrochim. Acta* **2013**, *96*, 274–284.
- (40) Mykhailiv, O.; Lapinski, A.; Molina-Ontoria, A.; Regulska, E.; Echegoyen, L.; Dubis, A. T.; Plonska-Brzezinska, M. E. Influence of the Synthetic Conditions on the Structural and Electrochemical Properties of Carbon Nano-Onions. *ChemPhysChem* **2015**, *16*, 2182–2191.
- (41) Plonska-Brzezinska, M. E.; Molina-Ontoria, A.; Echegoyen, L. Post-Modification by Low-Temperature Annealing of Carbon Nano-Onions in the Presence of Carbohydrates. *Carbon* **2014**, *67*, 304–317.
- (42) Mykhailiv, O.; Zubyk, H.; Brzezinski, K.; Gras, M.; Lota, G.; Gniadek, M.; Romero, E.; Echegoyen, L.; Plonska-Brzezinska, M. E. Improvement of the Structural and Chemical Properties of Carbon Nano-Onions for Electrocatalysis. *ChemNanoMat* **2017**, *3*, 583–590.
- (43) Szymański, G. S.; Wiśniewski, M.; Olejnik, P.; Koter, S.; Castro, E.; Echegoyen, L.; Terzyk, A. P.; Plonska-Brzezinska, M. E. Correlation between the Catalytic and Electrocatalytic Properties of Nitrogen-Doped Carbon Nanoions and the Polarity of the Carbon Surface: Experimental and Theoretical Investigations. *Carbon* **2019**, *151*, 120–129.
- (44) Plonska-Brzezinska, M. E.; Brus, D. M.; Breczko, J.; Echegoyen, L. Carbon Nano-Onions and Biocompatible Polymers for Flavonoid Incorporation. *Chem. - Eur. J.* **2013**, *19*, 5019–5024.
- (45) Bobrowska, D. M.; Czyrko, J.; Brzezinski, K.; Echegoyen, L.; Plonska-Brzezinska, M. E. Carbon Nano-Onion Composites: Physicochemical Characteristics and Biological Activity. *Fullerenes, Nanotubes, Carbon Nanostruct.* **2016**, *25*, 185–192.
- (46) Khorsandi, Z.; Metkazini, S. F. M.; Heydari, A.; Varma, R. S. Visible Light-Driven Direct Synthesis of Ketones from Aldehydes via

C H Bond Activation Using NiCu Nanoparticles Adorned on Carbon Nano Onions. *Mol. Catal.* **2021**, *516*, No. 111987.

(47) Schaetz, A.; Zeltner, M.; Stark, W. J. Carbon Modifications and Surfaces for Catalytic Organic Transformations. *ACS Catal.* **2012**, *2*, 1267–1284.

(48) Kuznetsov, V. L.; Chuvilin, A. L.; Butenko, Y. V.; Mal'kov, I. Y.; Titov, V. M. Onion-like Carbon from Ultra-Disperse Diamond. *Chem. Phys. Lett.* **1994**, *222*, 343–348.

(49) Guo, Y.; Wang, L.; Zhuo, J.; Xu, B.; Li, X.; Zhang, J.; Zhang, Z.; Chi, H.; Dong, Y.; Lu, G. A Pyrene-Based Dual Chemosensor for Colorimetric Detection of Cu²⁺ and Fluorescent Detection of Fe³⁺. *Tetrahedron Lett.* **2017**, *58*, 3951–3956.

(50) Zhang, R.; Tang, D.; Lu, P.; Yang, X.; Liao, D.; Zhang, Y.; Zhang, M.; Yu, C.; Yam, V. W. W. Nucleic Acid-Induced Aggregation and Pyrene Excimer Formation. *Org. Lett.* **2009**, *11*, 4302–4305.

(51) Andersson, O. E.; Prasad, B. L. V.; Sato, H.; Enoki, T.; Hishiyama, Y.; Kaburagi, Y.; Yoshikawa, M.; Bandow, S. Structure and Electronic Properties of Graphite Nanoparticles. *Phys. Rev. B* **1998**, *58*, 16387–16395.

(52) Rettenbacher, A. S.; Elliott, B.; Hudson, J. S.; Amirkhani, A.; Echegoyen, L. Preparation and Functionalization of Multilayer Fullerenes (Carbon Nano-Onions). *Chem. - Eur. J.* **2006**, *12*, 376–387.

(53) Vollmann, H.; Becker, H.; Corell, M.; Streeck, H. Beiträge zur Kenntnis des Pyrens und seiner Derivate. *Justus Liebigs Ann. Chem.* **1937**, *531*, 1–159.

(54) Hu, J.-y.; Hiyoshi, H.; Do, J.-H.; Yamato, T. Synthesis and Fluorescence Emission Properties of 1,3,6,8-Tetrakis(9H-Fluoren-2-Yl)Pyrene Derivative. *J. Chem. Res.* **2010**, *34*, 278–282.

(55) Murray, C.; Dozova, N.; McCaffrey, J. G.; FitzGerald, S.; Shafizadeh, N.; Crépin, C. Infra-Red and Raman Spectroscopy of Free-Base and Zinc Phthalocyanines Isolated in Matrices. *Phys. Chem. Chem. Phys.* **2010**, *12*, 10406–10422.

(56) Sun, B.; Dreger, Z. A.; Gupta, Y. M. High-Pressure Effects in Pyrene Crystals: Vibrational Spectroscopy. *J. Phys. Chem. A* **2008**, *112*, 10546–10551.

(57) Seoudi, R.; El-Bahy, G. S.; El Sayed, Z. A. FTIR, TGA and DC Electrical Conductivity Studies of Phthalocyanine and Its Complexes. *J. Mol. Struct.* **2005**, *753*, 119–126.

(58) Peak, D.; Luther, G. W.; Sparks, D. L. ATR-FTIR Spectroscopic Studies of Boric Acid Adsorption on Hydrous Ferric Oxide. *Geochim. Cosmochim. Acta* **2003**, *67*, 2551–2560.

(59) Ishihara, K.; Lu, Y. Boronic Acid–DMAPO Cooperative Catalysis for Dehydrative Condensation between Carboxylic Acids and Amines. *Chem. Sci.* **2016**, *7*, 1276–1280.

(60) Shiina, I.; Ushiyama, H.; Yamada, Y.; Kawakita, Y.; Nakata, K. 4-(Dimethylamino)Pyridine *N*-Oxide (DMAPO): An Effective Nucleophilic Catalyst in the Peptide Coupling Reaction with 2-Methyl-6-Nitrobenzoic Anhydride. *Chem. - Asian J.* **2008**, *3*, 454–461.

(61) Wang, Y.; Espenson, J. H. Efficient Catalytic Conversion of Pyridine *N*-Oxides to Pyridine with an Oxorhenium(V) Catalyst. *Org. Lett.* **2000**, *2*, 3525–3526.

(62) Wang, C.; Yu, H.-Z.; Fu, Y.; Guo, Q.-X. Mechanism of Arylboronic Acid-Catalyzed Amidation Reaction between Carboxylic Acids and Amines. *Org. Biomol. Chem.* **2013**, *11*, 2140–2146.

(63) Arkhipenko, S.; Sabatini, M. T.; Batsanov, A. S.; Karaluka, V.; Sheppard, T. D.; Rzepa, H. S.; Whiting, A. Mechanistic Insights into Boron-Catalyzed Direct Amidation Reactions. *Chem. Sci.* **2018**, *9*, 1058–1072.

(64) Lu, Y.; Wang, K.; Ishihara, K. Design of Boronic Acid-Base Complexes as Reusable Homogeneous Catalysts in Dehydrative Condensations between Carboxylic Acids and Amines. *Asian J. Org. Chem.* **2017**, *6*, 1191–1194.

(65) Petchey, T. H. M.; Comerford, J. W.; Farmer, T. J.; Macquarrie, D. J.; Sherwood, J.; Clark, J. H. Optimization of Amidation Reactions Using Predictive Tools for the Replacement of Regulated Solvents with Safer Biobased Alternatives. *ACS Sustainable Chem. Eng.* **2018**, *6*, 1550–1554.

(66) Siddiki, S. M. A. H.; Rashed, M. N.; Ali, M. A.; Toyao, T.; Hirunsi, P.; Ehara, M.; Shimizu, K. Lewis Acid Catalysis of Nb₂O₅ for Reactions of Carboxylic Acid Derivatives in the Presence of Basic Inhibitors. *ChemCatChem* **2019**, *11*, 383–396.

(67) Ghorpade, S. A.; Sawant, D. N.; Sekar, N. Triphenyl Borate Catalyzed Synthesis of Amides from Carboxylic Acids and Amines. *Tetrahedron* **2018**, *74*, 6954–6958.

(68) Sabatini, M. T.; Boulton, L. T.; Sheppard, T. D. Borate Esters: Simple Catalysts for the Sustainable Synthesis of Complex Amides. *Sci. Adv.* **2017**, *3*, No. e1701028.

(69) Gaudino, E. C.; Carnaroglio, D.; Nunes, M. A. G.; Schmidt, L.; Flores, E. M. M.; Deiana, C.; Sakhno, Y.; Martra, G.; Cravotto, G. Fast TiO₂-Catalyzed Direct Amidation of Neat Carboxylic Acids under Mild Dielectric Heating. *Catal. Sci. Technol.* **2014**, *4*, 1395–1399.

(70) Houlding, T. K.; Tchabanenko, K.; Rahman, M. T.; Rebrov, E. V. Direct Amide Formation Using Radiofrequency Heating. *Org. Biomol. Chem.* **2013**, *11*, 4171–4177.

(71) Lundberg, H.; Tinnis, F.; Adolfsson, H. Direct Amide Coupling of Non-Activated Carboxylic Acids and Amines Catalysed by Zirconium(IV) Chloride. *Chem. - Eur. J.* **2012**, *18*, 3822–3826.

(72) Hoang, L. T. M.; Ngo, L. H.; Nguyen, H. L.; Nguyen, H. T. H.; Nguyen, C. K.; Nguyen, B. T.; Ton, Q. T.; Nguyen, H. K. D.; Cordova, K. E.; Truong, T. An Azobenzene-Containing Metal–Organic Framework as an Efficient Heterogeneous Catalyst for Direct Amidation of Benzoic Acids: Synthesis of Bioactive Compounds. *Chem. Commun.* **2015**, *51*, 17132–17135.

Recommended by ACS

Liquid-phase Catalytic Continuous-Flow Aromatic Nitration Reactions with Conc. HNO₃ on Modified Mixed-Metal Oxide Composites as High-Yielding Solid Acid Catalysts

Haruro Ishitani, Shu Kobayashi, *et al.*

APRIL 04, 2023

ACS SUSTAINABLE CHEMISTRY & ENGINEERING

READ 

Ultrafine Ruthenium-Embedded P-Doped Carbon Materials as Bifunctional Catalysts for Solar-Assisted Water Splitting

Lin Hu, Zheng-hao Fei, *et al.*

JANUARY 11, 2023

ENERGY & FUELS

READ 

Ball-Milling-Enabled Zn(OTf)₂-Catalyzed Friedel–Crafts Hydroxyalkylation of Imidazo[1,2-*a*]pyridines and Indoles

Neha Meena, Anil Kumar, *et al.*

FEBRUARY 14, 2023

THE JOURNAL OF ORGANIC CHEMISTRY

READ 

Chitin Derived Carbon Anchored Ultrafine Ru Nanoparticles for Efficient Hydrogen Evolution Reaction

Enhui Ma, Deli Wang, *et al.*

NOVEMBER 11, 2022

ACS SUSTAINABLE CHEMISTRY & ENGINEERING

READ 

Get More Suggestions >